BASIN GEOCHEMICAL EVOLUTION OF THE EAGLE FORD AND EFFECTS ON TRACE ELEMENT RELEASE

A Thesis

by

IVAN MAULANA

Submitted to the Office of Graduate and Professional Studies of
Texas A&M University
in partial fulfillment of the requirements for the degree of

MASTER OF SCIENCE

Chair of Committee,	Michael Tice
Co-chair of Committee,	Bruce Herbert
Committee Members,	Franco Marcantonio
	Terry Wade
Head of Department,	Michael Pope

May 2016

Major Subject: Geology

ABSTRACT

The Ocean Anoxic Event 2 (OAE-2) at the Cenomanian-Turonian boundary is recognized from a carbon isotope excursion (CIE) in the Eagle Ford (EF) Group, and commonly attributed to global anoxic conditions in deeper marine settings. Whereas OAE are typically marked by widespread deposition of organic-rich shales, previous work shows diachroneity between the CIE and the organic-rich Lower EF, as well as anoxia-euxinia in the Western Interior Seaway of North America. We found evidence for periodic photic zone euxinia from an EF core, based on ratios of biomarkers and redox-sensitive trace elements. Sedimentary structures suggest depositional environments above storm wave base. Integration with a sequence-stratigraphic framework emphasizes the role of estuarine-style salinity stratification, subject to redox shifts caused by storm mixing in relatively shallow water depths. Independent zircon ages indicate that transition from the Lower to Upper EF occurs in the south before the north, consistent with a northward migration of this stratification mechanism as sea level rose. This implies that the redox states during deposition of the EF leading up to the CIE were influenced by regionally distinct mechanisms at relatively shallow water depths, instead of global anoxic conditions in deeper marine settings.

Euxinic shales are rich in trace elements, so there are high treatment costs to remove trace elements that have been released to matrix acidizing fluids during production, before these fluids can be disposed or reused. By understanding mechanisms controlling the interaction between euxinic shales and acidizing fluids, it may be possible to improve

the efficiency of unconventional production while simultaneously reducing environmental exposure. Trace element residency in and release from the EF were determined at different depths and under different temperatures and acid conditions. We found evidence that trace element release is mainly controlled by bulk trace element concentrations. This suggests that for the average rock, increased trace element release was associated with higher temperatures and acid concentrations, and these same conditions also resulted in higher sensitivity to trace element concentrations.

DEDICATION

To my family, country, and God for all the privileges I enjoy in life.

ACKNOWLEDGEMENTS

I would like to thank my committee chair, Dr. Michael Tice, for taking me under his wing, and for his guidance throughout the course of this project. I would also like to thank Dr. Terry Wade and Dr. Stephen Sweet at GERG for all the time and resources given to support my research. I sincerely appreciate my committee members for their time and feedback during my studies.

Thanks also go to my fellow graduate students, staff, and faculty of the Geology department, for making Halbouty my second home. I also want to extend my gratitude to the Berg-Hughes Center and the ConocoPhillips Fellowship for the academic resources and career opportunities.

Special thanks to Chip for your faith, confidence, and partnership.

NOMENCLATURE

AIR	Aryl Isoprenoid Ratio
CIE	Carbon Isotope Excursion
Cr	Chromium
Cr/Al	Chromium concentration
Cu	Copper
EF	Eagle Ford
Fe	Iron
GSB	Green Sulfur Bacteria
HCl	Hydrochloric acid
HST	Highstand Systems Tract
H_2S	Hydrogen Sulfide
ICP-MS	Inductively Coupled Plasma – Mass Spectrometry
MFS	Maximum Flooding Surface
Mn	Manganese
Mo	Molybdenum
Mo/Al	Molybdenum concentration
Ni	Nickel
OAE-2	Ocean Anoxic Event 2
OC	Organic Carbon
Pris/phy	Pristane/phytane ratio

SSD	Sequential Selective Dissolution
S	Sulfur
TE_{leach}	Amount of trace elements released in beaker leaching experiments
$TE_{original}$	Amount of trace elements present in original rock
$TE_{sulfide}$	Proportion of trace elements released from the sulfide fraction
TST	Transgressive Systems Tract
U	Uranium
V	Vanadium
WIS	Western Interior Seaway

TABLE OF CONTENTS

LIST OF FIGURES

LIST OF TABLES

1. INTRODUCTION

OAE-2 has been identified during a late-Cenomanian period of increasing organic carbon OC burial (Arthur et al., 1987; Jenkyns, 1980; Schlanger et al., 1987). A CIE of ca. 4‰ is globally observed, and has been attributed to shoreline transgression (Gale et al., 1993; Pratt, 1985). However, recent work has shown a decoupling between OC burial and the CIE in the Eagle Ford Group, suggesting a paradox of an oxygenated phase within OAE-2 (Eldrett et al., 2014). This paradox, however, assumes deposition of the Eagle Ford at more than 300 m water depth (Lock and Peschier, 2006; Ruppel et al., 2012). In contrast, a conflicting interpretation of the Eagle Ford's deposition at storm wave base (Donovan et al., 2012; Gardner et al., 2013) has been provided, which would suggest regional conditions distinct from the global anoxic conditions in deeper marine settings. Such regional conditions may better explain the decoupling of redox states and the CIE observed in the EF, and remove the apparent paradox. However, if a shallow water depositional model is applied to the EF, the development of euxinia would then need to be further explained. To better understand the redox states and depositional environment of the EF, and investigate the decoupling, we analyzed the Swenson-1H core located in the southern aperture of the WIS (Fig. 1.1).

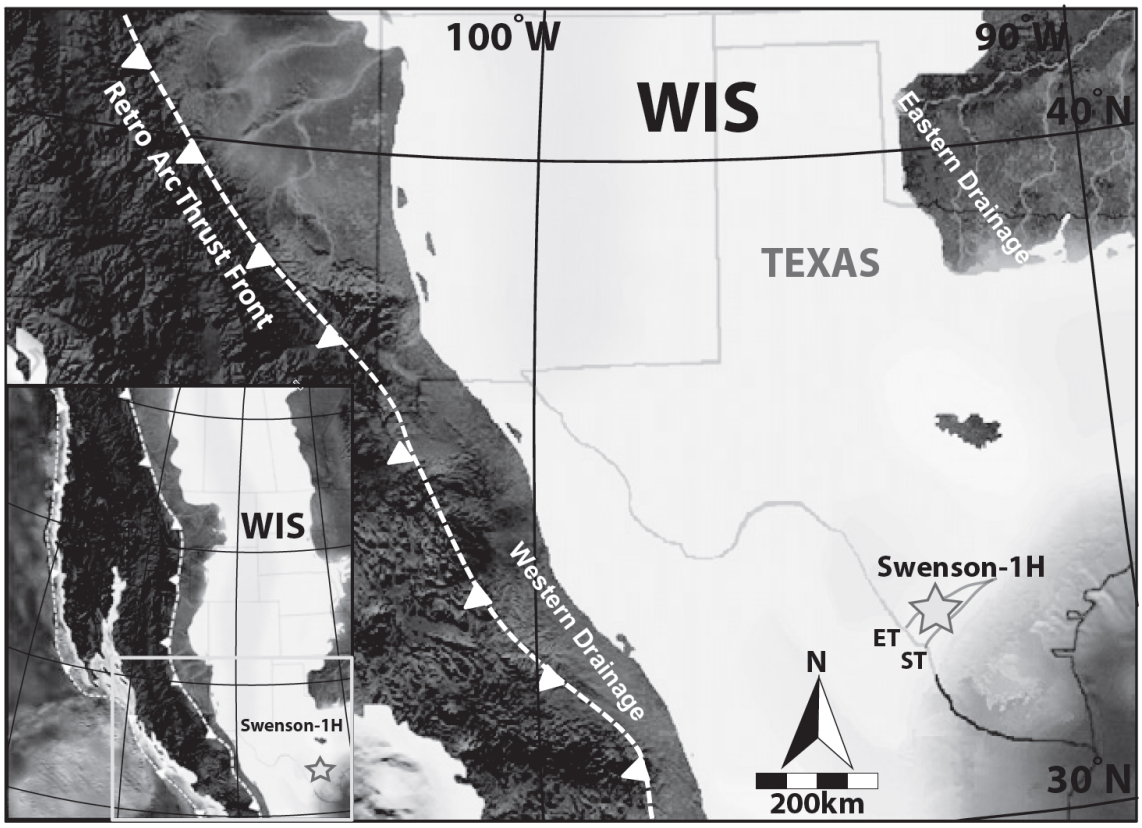

Figure 1.1. Paleogeography of the late-Cenomanian showing location of Swenson-1H core, modified from Eldrett et al. (2014), Ron Blakey and Colorado Plateau Geosystems, Inc. WIS – Western Interior Seaway; ET – Edwards Reef Trend; ST – Sligo Reef Trend.

1.1. Paleoenvironment and Geochemistry of the Eagle Ford

The EF was deposited between 100 - 86 Ma in the WIS, which was generated by enhanced accommodation in a retroarc foreland basin, together with eustatic rise from a pulse of rapid ocean crust formation (Hays and Pitman, 1973; Kerr, 1998; Schlanger et al., 1981). Transgression resulted in (1) creation of the Comanche Platform and its marginal Edwards reef trend updip from the Aptian Sligo reef trend rimming the Gulf of Mexico continental margin (Fig. 1.1); (2) increased OC production because warmer temperatures

and the flooding of continental shelves stimulated plankton production and nutrient cycling (Huber et al., 1995; 2002; Schlanger and Jenkyns, 1976). Anoxia, or euxinia if hydrogen sulfide is present, thus formed because of intensified oxygen uptake in organic debris decomposition, restricted circulation and longer residence times due to the rimmed margins, as well as decreased solubility in warmer waters (Donovan and Staerker, 2010; Donovan et al., 2012;). In addition, influx of freshwater from the eastern and western drainage basins in a humid climate limited vertical mixing and oxygenation in deeper waters (Jewell, 1993). Anoxia-euxinia in turn led to a decline in benthic foraminifera and bioturbation. This reduced remineralization and encouraged OC preservation (Elder, 1989; Gale et al., 2000; Jarvis et al., 1988).

1.2. Materials and Methods

The section of the Swenson-1H core (28.480701°N, 98.572305°W) studied consists of part of the EF, which is a carbonaceous calcareous mudstone. We (1) described the grain size, color, texture, lithology, and sedimentary structures of the core; (2) analyzed concentrations of redox-sensitive trace elements by X-ray fluorescence and inductively-coupled plasma mass spectrometry; (3) analyzed bulk organic carbon using LECO TOC and Rock-Eval pyrolysis; and (4) extracted and analyzed standard reference materials and powdered samples from the core at nine depths of interest for biomarkers, following Brocks et al. (2005) and Melendez et al. (2013). The enrichment patterns of molybdenum, uranium and chromium in different redox states is well-established and used to infer paleoredox states (Algeo and Maynard, 2004; Dahl et al., 2013; Tinnin et al., 2013; Tribovillard et al., 2004; 2006). Redox states influence the particle reactivity, solubility

and burial rates of these trace elements, so changes in their concentrations can be used to evaluate depositional conditions. Concentrations are normalized by aluminum, to correct for dilution by OC and authigenic minerals (Brumsack, 2006; Calvert and Pedersen, 1993; Morford and Emerson, 1999). Biomarker ratios of pristane (**I**), phytane (**II)**, and 2-alkyl-1,3,4-trimethylbenzenes (aryl isoprenoids; **III**) have been widely used to characterize anoxia or photic zone euxinia (Didyk, 1978; Grice et al., 2005; Summons and Powell, 1987). Aerobic decomposition produces more shorter-chain than longer-chain aryl isoprenoids. Phytol forms pristane by oxidation and decarboxylation under more oxic conditions. In contrast, anoxia-euxinia results in the dehydration of phytol to dehydrophytol and subsequent reduction to phytane. We calculated Pris/Phy and AIR (Schwark and Frimmel, 2004) for each sample.

1.3. Results and Discussion

Detailed dataset and results are in Appendix B. Sedimentary structures, log patterns, and elemental ratios were used to interpret a lithostratigraphic correlation to a sequence stratigraphic framework of the Eagle Ford (Donovan et al., 2012; Hildred et al., 2011). Six sub-units (A, B1 to B5) of the Lower EF Formation were recognized, and interpreted as two 4^{th}-order sequences consisting of transgressive and highstand systems tracts. A sharp decrease in OC occurs at 3165 m (Fig. 1.2), marking the contact of the organic-lean Upper EF. Production index and equivalent vitrinite reflectance calculated from Tmax (Table 1.1) suggest that the EF at this location is in the wet gas/condensate window.

TABLE 1.1. RESULTS OF GEOCHEMICAL ANALYSES OF NINE SAMPLES

Depth (m)	TOC (wt%)*	Carbonate (wt%)	Mo/Al[†]	Pris/Phy[§]	AIR[#]	C_{19} diaryl isoprenoid**	PI[††]	Re (%)[§§]
3164.2	2.68	54.22	2.7	0.45	1.83	81066	0.64	-
3166.9	3.58	36.84	21.5	0.38	1.68	174504	0.83	-
3172.2	4.18	60.59	19.3	0.60	1.98	442872	0.46	0.90
3175.3	1.86	84.41	20.2	0.57	2.95	231464	0.49	0.76
3177.3	5.41	63.61	42.6	0.46	3.43	77633	0.42	0.87
3178.7	1.12	92.14	43.7	0.40	2.15	-	0.49	0.83
3181.8	5.70	58.05	27.5	0.31	2.46	525474	0.48	1.03
3191.7	5.35	37.81	9.2	0.5	3.22	150272	0.52	0.92
3192.8	5.48	42.45	14.1	0.45	3.10	26500	0.57	0.78

*Total Organic Carbon
[†]Molybdenum concentration
[§]Pristane/phytane ratio calculated by Pristane/ (Pristane + Phytane)
[#]Aryl Isoprenoid Ratio(Schwark and Frimmel, 2004)
**Peak area of C_{19} diaryl isoprenoid
[††]Production Index
[§§]Equivalent vitrinite reflectance calculated from Rock-Eval Tmax measurements

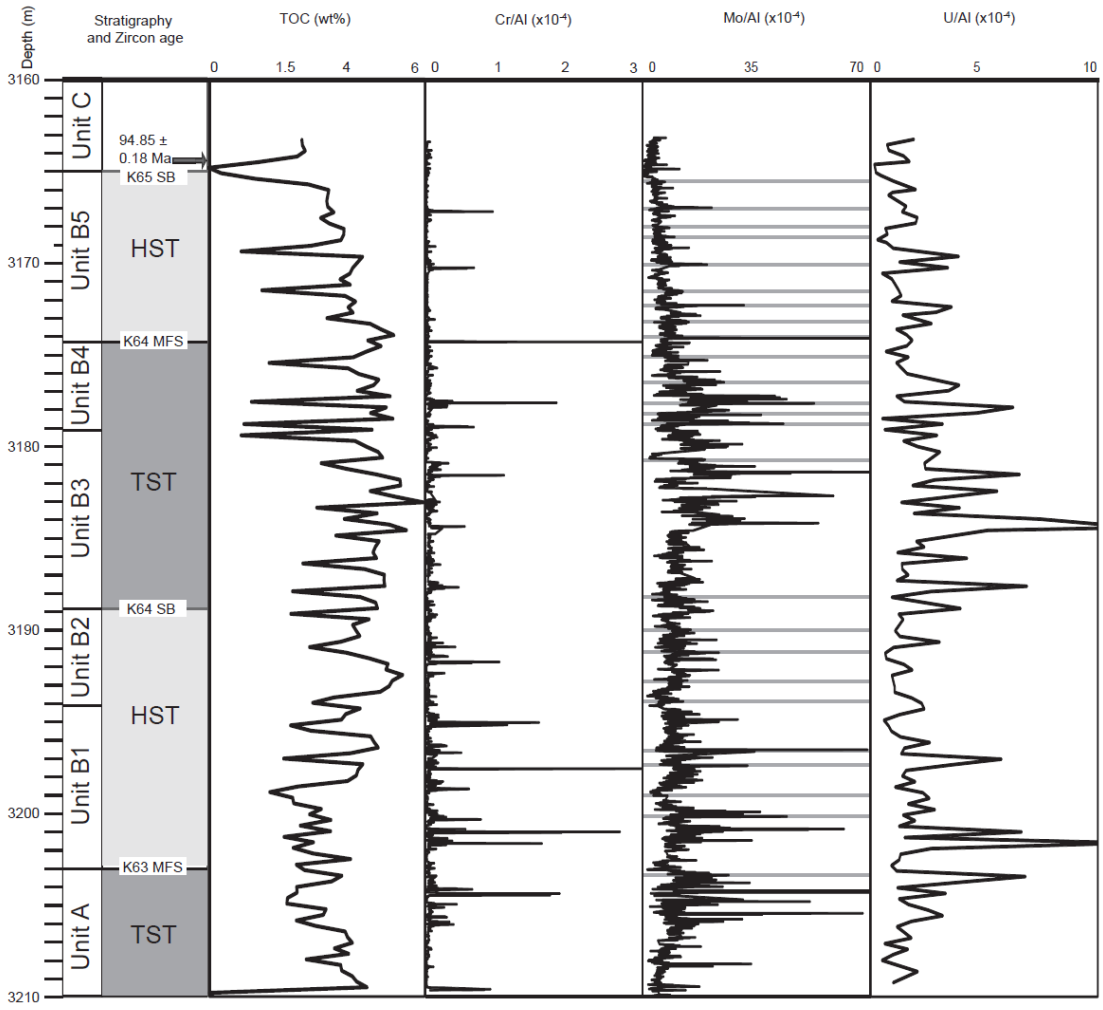

Figure 1.2. Results of Swenson-1H core from this study. A: Stratigraphy. Interpreted lithostratigraphic and sequence-stratigraphic units. Fourth-order sequences K63 and K64, and age of zircons from ash bed at 3164.4 m, are indicated. MFS – maximum flooding surface; SB – sequence boundary; TST – transgressive systems tract; HST – highstand systems tract. B. Total organic carbon (TOC; wt%). C: Chromium concentration (Cr/Al). D: Molybdenum concentration (Mo/Al) with visualized ash beds marked in grey. E: Uranium concentration (U/Al).

1.3.1. Paleoredox States

Pristane and phytane were identified in the saturated fraction of the organic extracts, and C_{13-22} aryl isoprenoids were identified in the aromatic fraction. The C_{17} aryl

isoprenoid was not observed, because the C_{16} and C_{18} homologues are more likely to be formed based on the branching pattern of irregular isoprenoids that have a tail-to-tail linkage. Pris/phy and AIR (Table 1.1) indicate periodic euxinia, consistent with data from a Webb County core (Fig. 1.3a; Romero, 2014). Mo/U ratios (Fig. 1.3b) are higher than average shale and approach that of modern seawater, suggesting that Mo and U deposition occurred equally effectively, meaning that a sulfidic environment must have existed to provide the required Mo burial mechanisms. Pristane, phytane, and aryl isoprenoids were also identified in the desulphurized polar fraction, consistent with the sulfurization of OC in a reducing environment during early diagenesis (Damste and de Leeuw, 1990; Damste et al., 1989). In addition to aryl isoprenoids, a homologous series of C_{19}-$_{23}$ 2,3,5',6-tetramethyl-2'-alkylbiphenyls (diaryl isoprenoids; **IV**) was also tentatively identified based on mass spectrum (Koopmans et al., 1996a). The C_{40} precursor of aryl isoprenoids, isorenieratane (**V**), was not observed probably due to the low proportion of isorenieratene (**VI**) that is preserved as free isorenieratane (<1%; Koopmans et al., 1996a). Furthermore, sedimentary rocks of high thermal maturity commonly contain isorenieratene breakdown products in the form of only aryl isoprenoids.

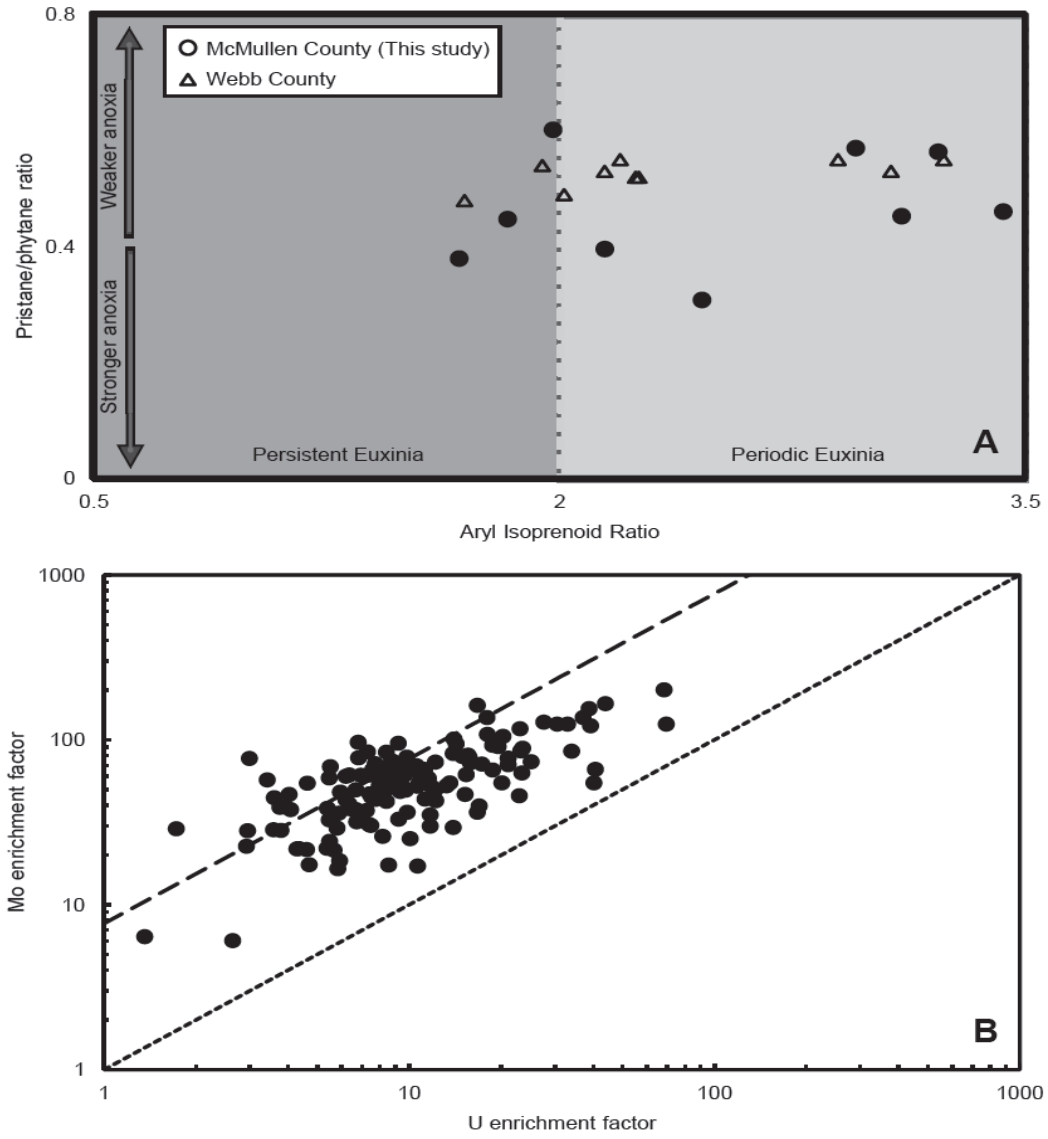

Figure 1.3. A: Crossplot of Aryl Isoprenoid Ratio on the horizontal axis and Pristane/Phytane ratios on the vertical axis. Aryl Isoprenoid Ratio was calculated according to Schwark and Frimmel (2004), and Pristane/Phytane ratios calculated by pristane/ (pristane + phytane). Circles are from this study, triangles indicate data from a Webb County core (Romero, 2014). B: Mo and U concentrations were normalized by average shale to calculate enrichment factors. Lines indicate constant Mo/U; dotted line – average shale; dashed line – seawater.

From 3194.3 – 3188.2 m, lower Mo and higher Cr concentrations (Fig. 1.2), with relatively high pris/phy, suggest a mostly anoxic environment without the presence of free H_2S. Conditions are interpreted as the most euxinic around 3182.1 m as Mo/Al reached a maximum, while pris/phy and AIR showed strong and persistent euxinia. Between 3182.1 m and 3176 m, there appeared to be a short episode of weak euxinia, transitioning into anoxia, based on the decrease in Mo/Al, and relatively high Cr concentrations (Cr/Al). This is interpreted as a period of shifting anoxia-euxinia as Mo/Al appears to spike and dip quickly while AIR suggests more periodic euxinia. Pris/phy at 3172.2 m also supports more oxic conditions.

From 3176 m, Mo/Al then suggest overall weakening euxinia, transitioning to anoxia, as shown by the broad decline in Mo/Al until 3170 m. This trend continues until the top of the core section. Coinciding with a brief and small maximum in Mo/Al at 3166.9 m, pris/phy and AIR suggest an episode of increased and relatively persistent anoxia-euxinia, nested within the general trend of decreasingly reducing conditions. However, the biomarkers demonstrate a degree of change in excess to that of Mo/Al. This may be because elemental indicators reflect mechanisms that can be active in the water column in the entire thickness of the euxinic zone, whereas molecular indicators are influenced by early diagenesis. A decoupling between elemental and molecular indicators can therefore suggest a thinner euxinic zone, where Mo/Al is enriched over a smaller settling distance, whereas diagenesis of biomarkers is unaffected by thickness of the euxinic zone.

The shallowest sample is interpreted to be in Unit C *sensu* Donovan et al. (2012), based on core lithology and a drop in Mo/Al to very low levels. This unit is also described

in Lozier Canyon to be bioturbated, suggesting oxygenation. The presence of mono- and diaryl isoprenoids, albeit at very low concentrations, thus appears to be contradictory. However, at this depth, there appears to be elevated Mo/Al, and lower Cr/Al, consistent with a possible euxinic episode. In addition, no burrows were interpreted at this depth of the core. Furthermore, the presence of diaryl isoprenoids is time-integrative as an accumulation of GSB cellular remains, and does not rule out oxygenated periods in shifting redox states.

1.3.2. Depositional Environment

Sedimentary structures interpreted as swaley and hummocky cross stratification suggest that the Eagle Ford was deposited at or above storm wave base. AIR that indicates periodic photic zone euxinia supports this inference, because influence from storm events would allow mixing of the water column, creating shifting redox states. Identification of the diaryl isoprenoids also supports this proposed depositional environment because the indicated photic zone euxinia means that anoxia-euxinia identified in the EF is not limited to a deep marine setting. Aryl isoprenoids are indicative because their precursor is isorenieratene, required for GSB photosynthesis under euxinic conditions (Koopmans et al., 1996a; Schaefle et al., 1977; Summons and Powell, 1986). Products of isorenieratene are identified by their characteristic 1,2,3,4 substitution pattern on the aromatic ring (Liaaen-Jensen, 1978). However, previous work has identified a possible diagenetic source of monoaryl isoprenoids from β-carotene (VII), a ubiquitous carotenoid (Koopmans et al., 1996b). During early diagenesis, the double bonds of β-carotene are hydrogenated before the cyclohexenyl moiety of β-carotane can be aromatized, followed by a geminal methyl

group shifting from the 3 to the 4 position, forming β-isorenieratane (VIII). C-C bond cleavage in the isoprenoid chain of β-isorenieratane can form monoaryl isoprenoids, interfering with the biological signal of GSB. The presence of photic zone euxinia can thus only be indicated if monoaryl isoprenoids are 15‰ enriched in $\delta^{13}C$, or if isorenieratene or its unique products can be identified. To this end, the identification of the series of aryl isoprenoids with a 1,2,3,4 substitution pattern and an additional aromatic ring requires the presence of isorenieratene. Formation of this additional aromatic ring requires first a *trans-cis* isomerization of one of the all-*trans* double bonds of isorenieratene (Koopmans et al., 1996a). Since β-isorenieratane does not have the required double bonds, an origin from β-carotene is ruled out. By contrast, an aryl isoprenoid with an additional aromatic ring, which has an origin from β-carotene, would have a 1,2,3 substitution pattern and a characteristic mass fragment of *m/z* 223, which is 14 Da less than that of an isorenieratene product (Koopmans et al., 1997).

1.3.3. Integration with Sequence-Stratigraphic Framework

To put the interpreted paleoredox states in geological context, we integrated the sequence-stratigraphic framework with the geochemical data. The HST of Unit B2 is interpreted where the geochemistry indicates increasingly reducing conditions. In the TST of Units B3 and B4, the trend of increasingly reducing conditions continues, but transitions into predominantly weak and shifting anoxia-euxinia at the MFS. In the subsequent HST of Unit B5, the suite of indices suggest minor episodes of anoxia-euxinia, nested within a general trend of less reducing conditions. Whereas a transgression was previously associated with anoxia-euxinia, our interpretation suggests that transgression resulted in

increased, then decreased euxinia. Reconciling these two trends emphasizes the role of a highly-stratified water column with limited vertical mixing (Bianchi, 1997), resulting in less diffusive and advective oxygen transport to the underlying saline water. In Unit B3, transgression led to the depletion of oxygen at depth from decomposition of sinking OC. In Unit B4, maximum flooding and estuarine mixing increased the amount of Tethyan water drawn under exported freshened water, causing northward migration of the shoreline and halocline (Fig. 1.4). This would in turn lead to improved ventilation, explaining the bidirectional trend during the interpreted TST. By contrast, if anoxia-euxinia was solely controlled by oxygen depletion creating a chemocline at depth, and related to global anoxic conditions in deeper marine settings, then transgression would be accompanied simply by more reducing conditions. Another alternative mechanism is transgression resulting in a thermocline, improving oxygen solubility in colder waters. However, this is unlikely as water depths of more than 300 m are required for a thermocline to develop, contradicting with the interpreted depositional environment.

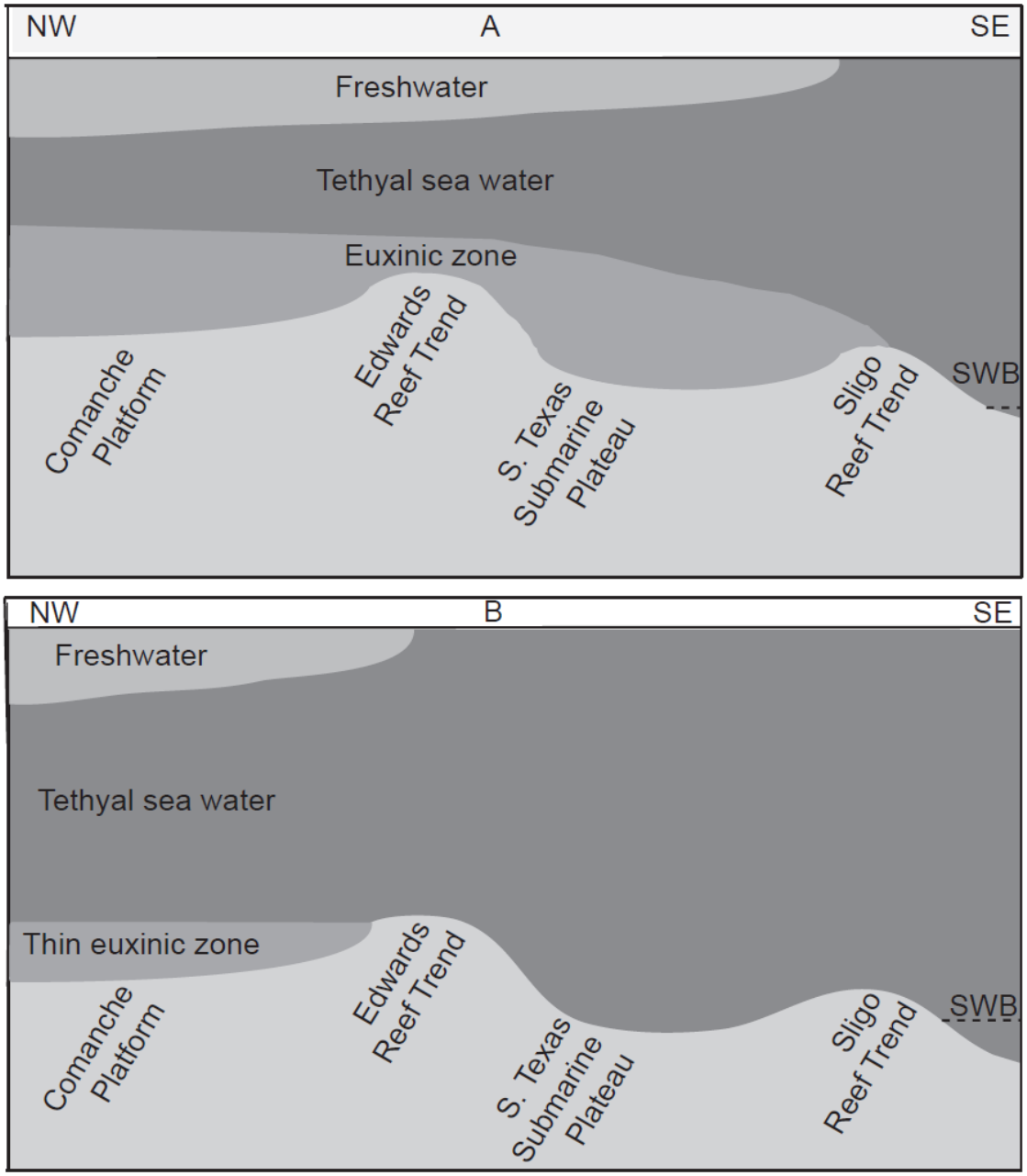

Figure 1.4. Schematic of evolution in water column stratification and paleoredox states across a northwest-southeast transect over the Edwards and Sligo reef trends, modified from Bianchi (1997) and Donovan et al. (2012). A: Initial transgression. B: Maximum flooding. SWB – storm wave base.

In the HST of Unit B5, sea level is expected to fall, and stratification to increase again. Pris/phy and AIR suggest euxinia comparable to Unit B3. However, Mo/Al suggests much weaker euxinia, and shows similar concentrations to the previous HST. As discussed earlier, this divergence between molecular and elemental indices can be due to the trace elements recording a smaller cumulative effect in a thinner euxinic zone, with more of the water column being oxygenated even with water bottom euxinia. This suggests that freshwater stratification may not yet have been restored to the original extent, that marine waters drawn into WIS had improved connection and sustained mid-column oxygenation, that the productivity effects of initial shelf transgression was absent, or a combination of the three.

Migration of the shoreline and chemocline northward is independently supported by zircon dating ages, which have identified that the contact between the Upper and Lower EF is younger in the northwest than in the southeast (Pierce, 2014). At this core location, the OAE-2 happened at the turn of the Cenomanian-Turonian transgressive-regressive cycle, when sea levels were at the highest regional highstand of the Phanerozoic (Hancock and Kauffman, 1979; Haq et al., 1987). This means that the shoreline, haloclines and chemoclines would have migrated furthest north, allowing ventilation at this location, providing regional controls on the decoupling of OC preservation in the EF from the global CIE. Such an oxygenated phase and the resulting poorer OC preservation would also account for the relatively organic-lean Upper EF. I propose that the presence of this "diminished stratification" mechanism, in relatively shallow water depths, would explain the oxygenated phase occurring during the OAE-2 identified by Eldrett et al. (2014).

Application of a shallow water depositional model for the EF would thus remove Eldrett's paradox of oxygenation in a deepwater setting. Conversely, a shallow water model for the EF would instead suggest a need for wider study on the development of the anoxic-euxinic shallow water paleoenvironment, and on the development of contributing mechanisms such as water column stratification.

2. TRACE ELEMENT RESIDENCY AND RELEASE

Matrix acidizing is a distinct process from hydraulic fracturing that involves using acid to increase permeability within 20' of the wellbore. HCl is injected at a relatively low pressure to create highly conductive flow channels ("wormholes") as the acid dissolves carbonates. These wormholes then allow fracturing fluids to enter deeper into the formation (Economides et al., 2013). As the rock is being dissolved, trace elements enriched in the formation can are released to the acidizing fluids. High concentrations of dissolved trace elements in the flowback acidizing fluid can result in high salinity (total dissolved solids), requiring high treatment costs before water reinjection or disposal can be done (Guerra et al., 2011). By understanding mechanisms controlling the interaction between euxinic shales and acidizing fluids, it may be possible to engineer higher efficiency of unconventional production while simultaneously reducing environmental exposure.

Trace element residency was analyzed using SSD, to identify the amounts of trace elements released separately from each of the four major extractable fractions within the formation (exchangeable, organic, carbonate, sulfide). Different reactants are used to mobilize trace elements from each fraction (Fig. 2.1). Each extractable fraction has a different level of stability, and the partition of trace elements between these extractable fractions is determined by depositional redox conditions. $TE_{original}$ is expected to consist of these four extractable fractions, together with a nonextractable fraction of oxides and silicates.

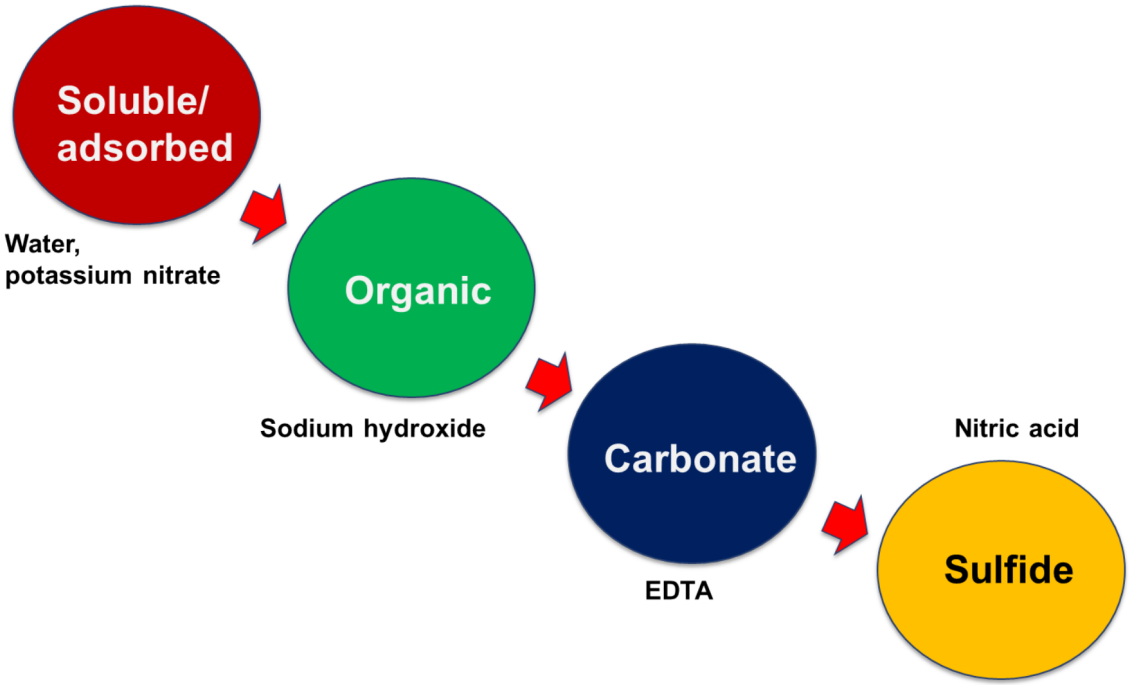

Fig 2.1. Schematic showing the four fractions in which trace elements reside in the samples, and the corresponding reactants used to mobilize each fraction in the sequential selective dissolution process. EDTA - disodium ethylenediaminteraacetic acid.

A simple model (Fig. 2.2) of the controls on trace element release to acidizing fluids was created to include six factors: $TE_{original}$, trace element residency, lithofacies, surface area, the concentration of acid used, and kinetic factors based on formation temperature. This is a static model that does not account for mass transport. Trace element release was analyzed by leaching the nine depth samples with HCl under reservoir conditions. By correlations of the amount of released trace elements with the six variables, I identified the dominant controlling mechanisms from the simplified model.

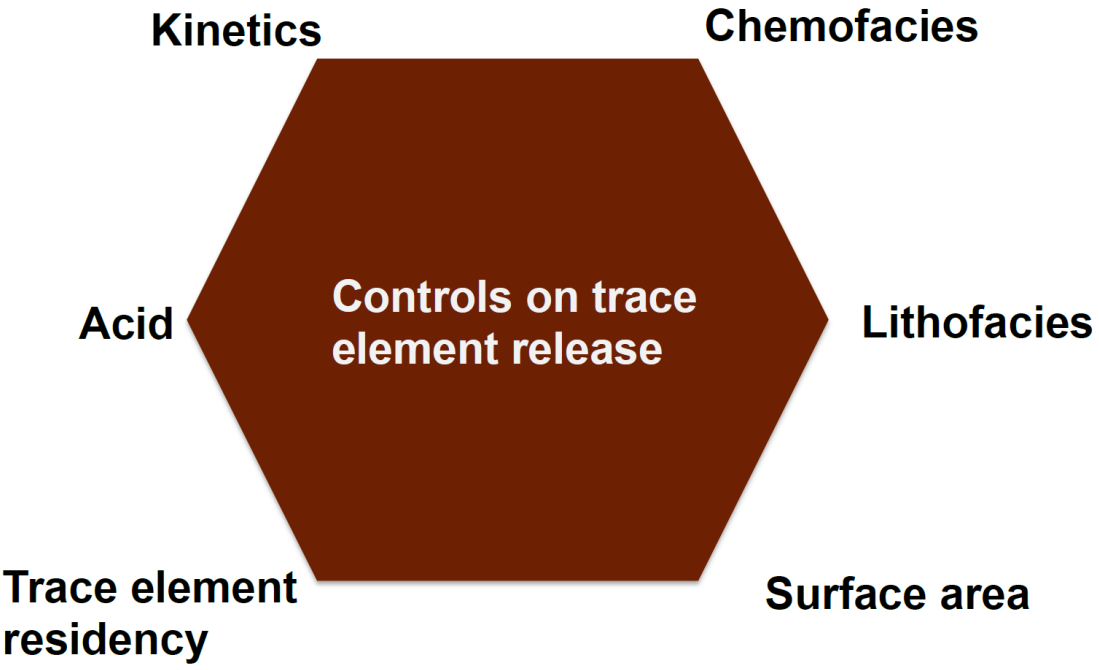

Figure 2.2. Schematic showing conceptual model of controls on trace element release.

2.1. Trace Element Geochemistry

Anoxic sulfate reduction releases H_2S, which readily forms sulfide minerals that remove most trace elements. Trace elements associated with sulfides have been reduced to their thermodynamically favored lowest valence state, and are typically stable with little or no confounding diagenetic effects, resulting in their enrichment in euxinic facies. The associative behaviors of six redox-sensitive trace elements are described in this section, with examples illustrated in a redox ladder (Fig. 2.3).

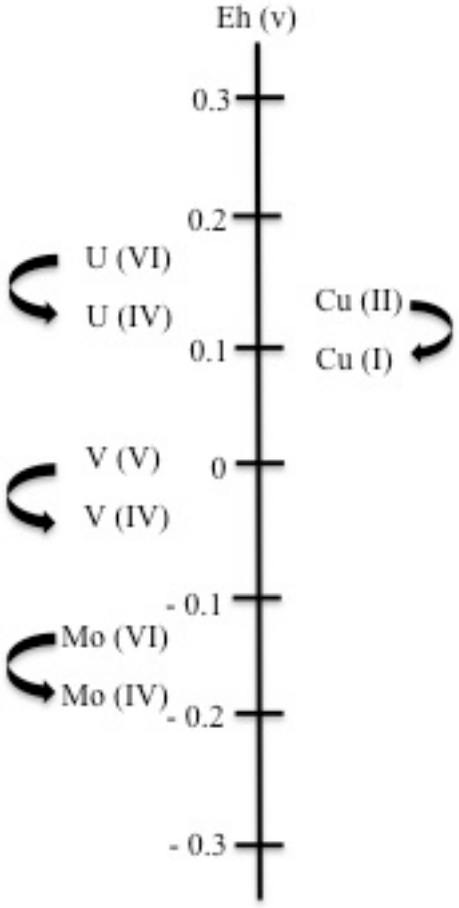

Figure 2.3. Redox ladder showing examples of trace element species at pH 7.

2.1.1. Uranium

U is often well correlated to OC concentrations in anoxic facies. Under oxic conditions, conservative uranyl ions (UO_2^{2+}) form a strong complex with carbonate ions (Anderson et al., 1989). Under reducing conditions or lower pH, uranyl is reduced to UO^{2+}, and can be stabilized by humic acids, forming organometallic complexes, or precipitated as uraninite (UO_2) or its precursors. Reduction and precipitation to stable forms occur predominantly in sediments and is primarily influenced by uranyl carbonate diffusion from

the water column, under low sedimentation rates, unless the water column itself is anoxic (Chaillou et al., 2002; Klinkhammer and Palmer, 1991; McManus et al., 2005). No sulfides are expected to be formed because UO^{2+} is a class A Lewis hard acid, and OH^- readily displaces sulfide species.

2.1.2. Vanadium

The stepwise reduction of V makes it a particularly good way of indicating small redox variations. V is present in the oxic water column as vanadate oxyanions (VO_4^{3-}; Wehrli and Stumm, 1989). In reducing conditions, it is reduced to vanadyl (VO^{2+}) hydroxides, or adsorbed to humic and fulvic acids, forming organometallics. No sulfides are expected to be formed because VO^{2+} is a class A Lewis hard acid, and OH^- readily displaces sulfide species. In sulfidic conditions, further reduction to V^{3+} occurs, which precipitates as sulfides, oxides, or chelates porphyrins (Breit and Wanty, 1991; Emerson and Huested, 1991; Wanty and Goldhaber, 1992).

2.1.3. Molybdenum

Mo in oxic conditions is mainly present as molybdate (MoO_4^{2-}) or adsorbed to Fe/Mn oxyhydroxides, and is repartitioned via three processes. First, oxygen atoms in molybdate can be replaced by soft ligands such as sulfur donors, covalently bonding molybdate with macromolecular detritus. Alternatively, persistently sulfidic conditions with proton donors and active surface minerals catalyze the formation of thiomolybdates (MoS_4^{2-}), which have particle-reactive surface groups and are prone to scavenging by pyrite or organic particles. With pyrite, it forms Mo-Fe-S cuboidal clusters, stabilizing the structure. Lastly, it can also form insoluble MoS_2 (Crusius et al., 1996; Erickson and Helz,

2000; Helz et al., 1996; Vorlicek and Helz, 2002; Vorlicek et al., 2004). Pyrite co-precipitation occurs at sulfide concentration of ~0.05μM, whereas particle association occurs at a second threshold of ~100μM (Zheng et al., 2000). Higher Mo concentrations can thus be used to interpret euxinic conditions.

2.1.4. Chromium

Cr is present in oxic conditions as soluble chromate (CrO_4^{2-}), and is reduced to aquahydroxyl [$Cr(H_2O)_4(OH)_2^+$] or hydroxyl [$Cr(OH)_2^+$] in anoxic waters, which then precipitate at high pH. At low pH, these cations can also be insoluble as they complex with organic acids or adsorbed to Fe/Mn oxyhydroxides. However, the uptake by pyrite of Cr(III) is negatively affected by structural and electronic incompatibility. Thus in euxinic conditions, as sulfide reactions occur, Cr may be remobilized from sediments, and lower concentrations are expected. Cr often has a detrital provenance, which needs to be considered when reconstructing paleoenvironments.

2.1.5. Nickel

Ni is present in oxic waters as Ni^{2+} or adsorbed to humic and fulvic acids in organometallics. Ni is more readily oxidized than Cu, and may be released to pore waters upon OC decay. In anoxic conditions, Ni can be cycled from sediments to the water column due to the absence of sulfides and Mn oxides, but generally remain in organometallics. In euxinic conditions, Ni readily chelates porphyrins. It also forms sulfides at a kinetically slower rate, limiting its concentration in authigenic minerals (Grosjean et al., 2004; Huerta-Diaz and Morse, 1990; 1992; Lewan and Maynard, 1982; Morse and Luther, 1999).

2.1.6. Copper

Cu in the form of Cu^{2+} is scavenged from oxic waters into organometallics or adsorbed onto particulate Fe/Mn oxyhydroxides (Fernex et al., 1992; Sun and Puttmann, 2000). Under euxinic environments, it is released and reduced to Cu^{+}, then incorporated into pyrite or sulfides. Under sufficiently low sedimentation rates, Cu is also fixed by smectite (Pedersen et al., 1986).

2.2. Materials and Methods

Nine depth samples were selected from the core, making sure that samples represented different carbonate content, multiple stratigraphic positions (Units B2 to C), and a wide range of Mo/Al indicating different redox conditions. The grain sizes of powdered samples obtained using a hand drill were determined by visualization under a microscope, before measuring 300 random grains using a 30μm rectangular grid. Measured grain sizes are shown in Appendix B.

2.2.1. Sequential Selective Dissolution

SSD (Sullivan and Yelton, 1988) was used to sequentially mobilize soluble/adsorbed, organic-bound, carbonate and sulfide fractions of trace elements. A sequence of reagents of increasing chemical reactivity was used to target each of the fractions. 2g of each sample were weighed out in 50ml centrifuge tubes, as well as one blank. Trace elements in the soluble fraction were mobilized by adding 25ml 0.5M potassium nitrate, shaken, and allowed to rest for 16 hours. Samples were then centrifuged at 6000rpm for 22 minutes, and the supernatant liquid decanted and retained for ICP-MS analysis. The adsorbed fraction was mobilized by deionized water for 2 hours three times

and combined with the potassium nitrate. The organic-bound fraction was mobilized using 0.5M sodium hydroxide for 16 hours. The carbonate fraction was mobilized with 0.05M disodium ethylenediaminteraacetic acid for 6 hours, while 4M nitric acid was used for the sulfide fraction at 80°C for 16 hours.

2.2.2. Trace Elements Mobilized by Leaching in Beakers

Samples were leached with HCl in anaerobic conditions using sealed serum bottles inside an anaerobic glove box. Each sample was leached at three different temperatures using three acid concentrations, for a total of nine times. The same mass of powdered sample was placed in each bottle, enough to be spread out in a thin layer over the bottom of the bottle (Fig. 2.4). The three concentrations of HCl were determined by using 15% acid by mass, which is common in industry, as the maximum. The high and low acid concentrations were two orders of magnitude higher and lower, respectively, in order to have range of pH values. The samples were acidified with a constant 10:1 mass ratio of acid to powdered sample. Three samples of 20:1 mass ratio were also added to control for the effect of different acid amounts. Samples were acidified in an anaerobic environment and immediately sealed.

Figure 2.4. Photograph of powdered samples in thin layer over the bottom of serum bottles prior to sealing.

Since reaction rates vary as an inverse of temperature, a non-linear range of temperatures (20, 65, 120°C) was used to allow a linear spread of values. The run time for all the samples was 1 hour, which is a common residence time for matrix acidizing in the formation before being pumped out. The 65°C run was conducted in a water bath, while the 120°C run was conducted in an autoclave oven (Fig. 2.5).

Figure 2.5. Photograph of serum bottles in autoclave oven before 120°C run.

At the end of each run, the samples were returned to an anaerobic glovebox, and a syringe with filter was used to retrieve a colorless fluid from the sample bottles. This fluid was retained for ICP-MS analysis, to determine TE_{leach}.

2.2.3. Trace Element Quantification

Concentrations of the six trace elements mobilized in the SSD and leaching experiments were analyzed on an ICP-MS. Four dilutions of an analytical standard were used to create a regression. Samples were injected into the ICP-MS and quantified in relation to the analytical standard. We used a Single Collector High Resolution ICP-MS Thermo Element XR, which has resolving power up to 10,000. For this study, low and medium resolutions with resolving powers of 300 and 4000 respectively were used. Isotopes measured in low

resolution were ^{55}Mn, ^{98}Mo, ^{187}Re, ^{238}U, and ^{232}Th, consisting of 40 samples per peak, with a mass window of 10 and an integration window of 80. Isotopes measured in medium resolution were ^{56}Fe, ^{63}Cu, ^{51}V, ^{60}Ni, and ^{52}Cr, consisting of 20 samples per peak, with a mass window of 100 and an integration window of 60. Analysis was operated at an RF power of 1250W, sample uptake rate of 100 µl/min, acquisition time of 60 s, wash time of 90 s, in electric scanning acquisition mode and triple detection mode.

2.3. Results and Discussion

Results of SSD analysis are shown in Table 2.1, and detailed ICP-MS results are listed in Appendix B. ICP-MS analyses of SSD samples showed that 65 – 90% of the trace elements were released from the sulfide fraction, with an average of 91% and a median of 94%. This significant association with sulfide minerals is consistent with the presence of anoxia-euxinia. At the lowest end, only 65% of Mo being released from the sulfide fraction is consistent with the idea of weak euxinia.

A comparison between trace elements released from SSD and a complete digestion showed that the SSD method resulted in an average of 80% of total trace elements being released. This is the environmentally-relevant or bio-available fraction present in each sample, and can be taken to be representative of the total amount present. Results from the leaching experiments showed that the duplicates differed by an average of 1.3%. When the mass of acid added to powdered samples during the leaching experiment was doubled, no significant change was found, with results differing by an average of 0.2%.

TABLE 2.1. RESULTS FROM NINE DEPTH SAMPLES

Depth (m)	Grain size (μm)	Total concentration released from Sequential Selective Dissolution (μg/g)						Total Mo concentration released from complete digestion (μg/g)
		Molybdenum	Uranium	Copper	Vanadium	Nickel	Chromium	
3164.2	0.62	2019.335	1623.064	846.4281	47615.89	17808.27	29364.25	6776.827514
3166.9	1.41	22352.35	3030.184	1091.802	260511.6	41741.83	38771.13	25898.09955
3172.2	1.17	22966.66	3867.406	1060.603	166735.9	27320.11	38619.92	28492.1488
3175.3	1.19	26196.73	3026.083	1632.852	288570.4	49508.27	86099.64	29879.00626
3177.3	1.04	31280.13	9252.685	1676.941	258873.2	51410.46	89676.62	37741.90265
3178.7	1.05	31404.83	4447.168	1729.328	161072.1	65005.15	44925.77	34836.97123
3181.8	1.47	31955.38	6939.01	1211.068	275124.8	70308.18	37208.43	35505.16602
3191.7	0.68	4779.809	1468.259	592.1706	72766.32	15165.26	27120.32	6451.814338
3192.8	1.11	30950.87	3400.521	1570.251	109578.4	42654.26	30376.38	35384.04309

Even though anoxia-euxinia is expected to correlate with elevated $TE_{sulfide}$, consistently high $TE_{sulfide}$ from this study was not sensitive to the redox indices, and was higher than expected for a given value of a redox index (Fig. 2.6; Anova regressions P-values > 0.07). There are four possible reasons for this observation. First, as reducing conditions start being established, a progressively larger fraction of trace elements were rapidly scavenged by sulfides. In other words, almost all the trace elements stored was already in the sulfide fraction. However, when the amount of trace elements in the other fractions approaches zero, an increase in trace elements stored in sulfides will have little numerical effect on $TE_{sulfide}$. Second, trace elements are enriched under reducing conditions in stepwise orders of magnitude. A single relationship should not be expected between $TE_{sulfide}$ and Mo/Al. In this case, however, the sample points do not appear to fall into different clusters. Third, a larger sample population over a wider range of values would better resolve the evolution of $TE_{sulfide}$ with the redox indices. Lastly, trace element residency may not correlate with molecular redox indices if there were different redox conditions at the water bottom compared to the water column. Since speciation in sediments can by extension be independent of the overlying water column, trace element residency may not be predicted by seawater chemistry.

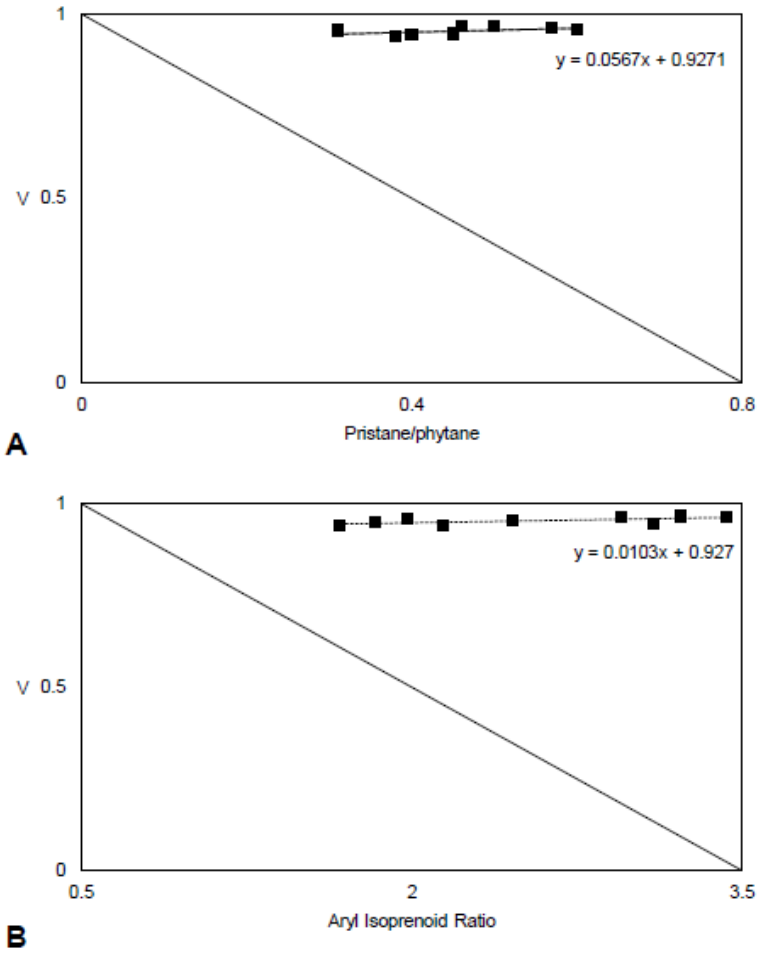

Figure 2.6. Proportion of redox-sensitive trace element released from the sulfide fraction plotted as a function of A: Pristane/phytane ratio and B: Aryl Isoprenoid Ratio. V – Proportion of vanadium in sulfide fraction; the solid line is the line of proportional increase.

TE_{leach} of each sample was normalized by the respective grain sizes, to control for surface area effects on trace element release. Trace elements in the sulfide fraction are expected to be more stable, but there was little correlation between normalized TE_{leach} and $TE_{sulfide}$ when I plotted the two parameters (Anova regressions P-values > 0.1). This

suggested that trace element residency was not a major control of TE_{leach} during the matrix acidizing process. Normalized TE_{leach} had little correlation with carbonate content either (Anova regressions P-values > 0.08), suggesting that lithofacies was not a major control of TE_{leach}.

Principal components analysis was carried out using concentrations of each element released from each of the soluble, organic, carbonate and sulfide fractions. Among three principal components, Anova regression showed that Principal Component 1 (PC1) had the most statistically significant relationship with normalized TE_{leach} under all experimental conditions and for all six elements. PC1 represented a weighted magnitude parameter of trace element concentrations in the rock, i.e. $TE_{original}$, and explained between 24% - 88% of the variation in the data. A significant relationship was found for the elements Mo and V when normalized TE_{leach} was plotted against PC1 (Fig. 2.7; median R^2= 0.5, Anova regressions P-values < 0.05). Positive coefficients demonstrate that normalized TE_{leach} is controlled by $TE_{original}$, the bulk concentration of trace elements. P-values for U, Cu, Ni and Cr were >0.06 possibly because of low analytical confidence due to low concentrations. It may also be a result of their weaker euxinic affinity (Algeo & Maynard, 2004), meaning that they have lower enrichment in euxinic facies. As a result, the effects of PC1 on normalized TE_{leach} are expected to be smaller, and would have a signal that is easily interfered with by any other factors affecting TE_{leach}. Furthermore, PC1 in these results is a vector that ranges only from -2 to 2, so small numerical variation in PC1 represents a large amount of actual change. Differences in trace element residency are not expected to be responsible for the high P-values of the regressions for Cu and Ni,

because they are also stored in sulfides, similar to Mo and V. Regressions of U have P-values similar to Cu, Ni, and Cr, probably due to its relatively low concentrations. This is not expected because it has a higher euxinic affinity than Mo and V, but may also be attributed to post-depositional loss in a shallow water environment subject to storm mixing.

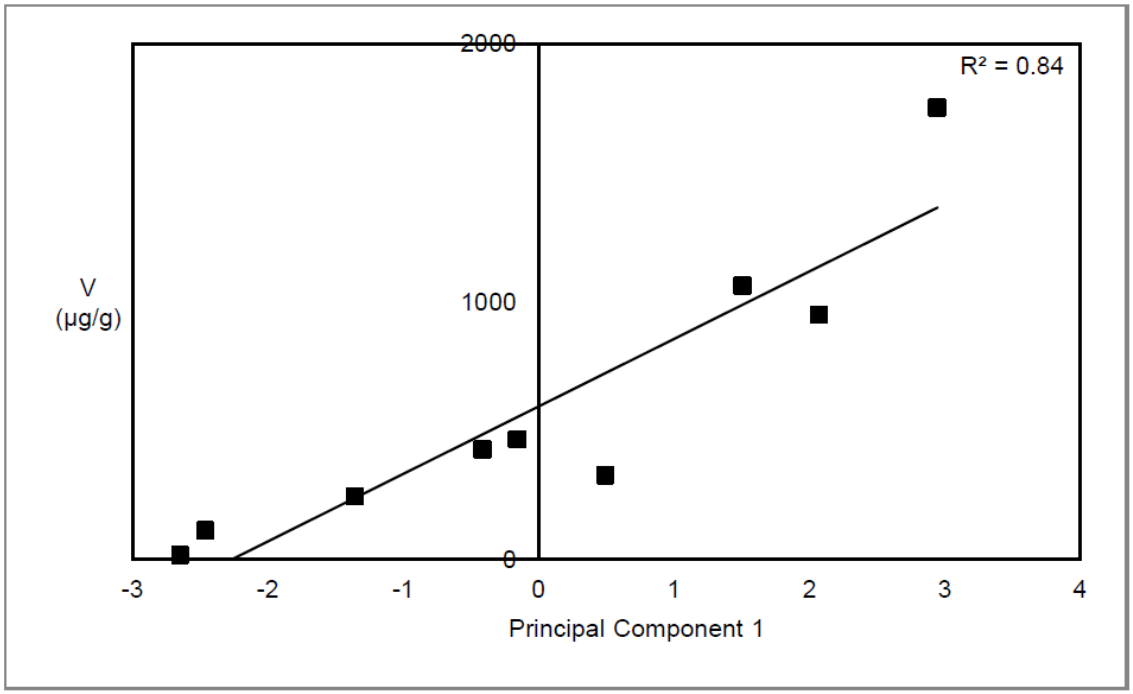

Figure 2.7. Concentration of redox-sensitive trace element released during leaching in beaker experiment plotted against Principal Component 1. Example from 20°C and 0.0015% HCl experiment. V - Concentration of vanadium (µg/g) released during leaching in beaker experiment, normalized by grain size of powdered samples.

Even though different redox states are expected to affect trace element concentrations, PC1 and normalized TE_{leach} had weak correlations with Pris/phy, AIR, and

Mo/Al (Anova regressions P-values > 0.06). The lack of correlations with the redox indices in this study can again be attributed to one or more of the five reasons earlier discussed.

Plots of the coefficients and intercepts for each of the regressions according to varying temperatures and acid concentrations (Fig. 2.8) show that the intercepts and coefficients had two distinct populations; results from the 15% acid experimental conditions or the 0.15% acid and 120°C experiment were very different from the five other experiments. The coefficients represent the sensitivity of TE_{leach} to PC1 and the intercepts represent TE_{leach} of the average rock. The presence of the different populations suggest that the average rock released more trace elements under higher temperatures, or under acidizing fluids of higher acid concentrations. In addition, the coefficients suggested that the higher the temperatures and acid concentrations, the higher the sensitivity to varying trace element concentrations.

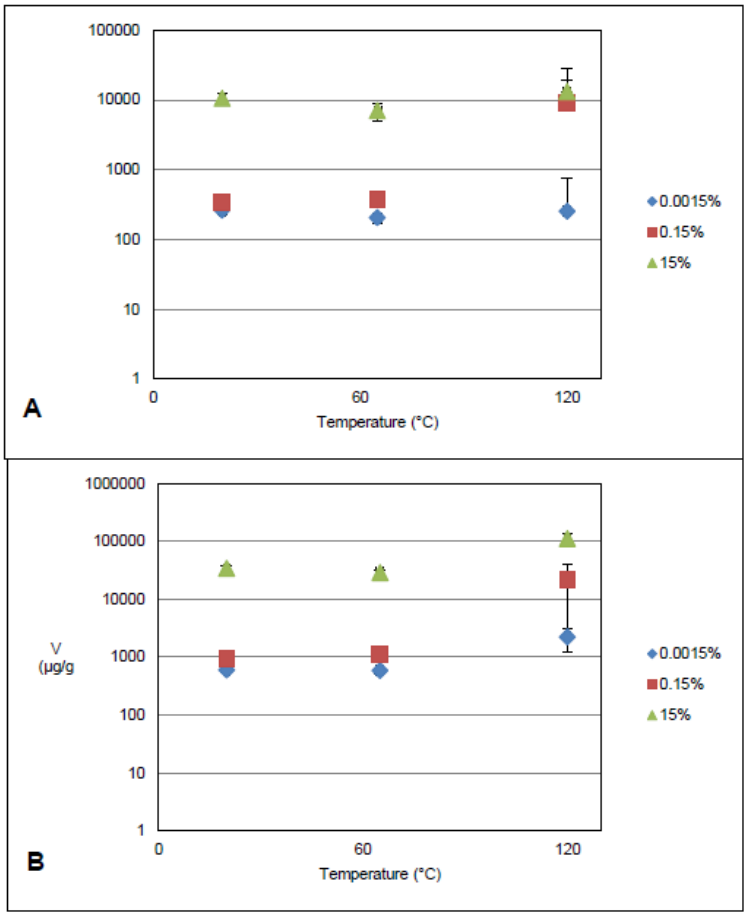

Figure 2.8. Plots of A: Coefficients and B: Intercepts from Anova regressions of Principal Component 1 with redox-sensitive trace element released during leaching in beaker experiment. V - Concentration of vanadium (µg/g) released during leaching in beaker experiment, normalized by grain size of powdered samples.

These interpretations have engineering implications because they argue for matrix acidizing fluids to have the highest practicable pH. Currently, acetic and formic acids are sometimes used as alternatives to HCl because stronger acids are spent too quickly and stimulate permeability less effectively, while some workers have also sought to develop alternatives with slower reaction rates (Markey, 2014). The results from this study provide

further justification for matrix acidizing fluids with lower reaction constants, and this becomes even more imperative if the target formation is known to have a high bulk concentration of trace elements.

3. CONCLUSION

Low pristane/phytane ratios support the presence of anoxic conditions during deposition of the Eagle Ford, whereas high Aryl Isoprenoid Ratios suggested that euxinic conditions were intermittent. The presence of pristane, phytane, and aryl isoprenoids in the desulphurized polar fraction agreed with the sulfurization of OC in a reducing environment during early diagenesis. Mo/U ratios approach that of standard seawater, suggesting that euxinic conditions were present to enhance Mo burial efficiency comparable to that of U. The interpretation of intermittent euxinia and hummocky sedimentary structures are consistent with a depositional environment at storm wave base. Tentative identification of diaryl isoprenoids are diagnostic of photic zone euxinia, which means that deposition of the Eagle Ford cannot be constrained to a deepwater environment. Integration of the trace element concentrations within a sequence-stratigraphic framework implicates the presence of a salinity stratification mechanism that prevented oxygen transport. Migration of the halocline with changing sea levels is proposed as an explanation for regional decoupling of organic carbon burial with a carbon isotope excursion.

65-90% of the six studied trace elements were stored in the sulfide fraction at nine sample depths of the Lower Eagle Ford core. No significant relationship was found between redox conditions, trace element residency, and the amount of trace elements released under simulated production conditions. Rather, the release of trace elements with high euxinic affinity was significantly influenced by bulk concentrations. This relationship was less significant for trace elements with low euxinic affinity. Higher reservoir

temperatures and acid concentrations were found to elevate trace element release, and this effect was amplified when original bulk concentrations of trace elements were higher.

REFERENCES

Algeo, T. J., and Maynard, J. B., 2004, Trace-element behavior and redox facies in core shales of Upper Pennsylvanian Kansas-type cyclothems: Chemical Geology, v. 206: 289-318.

Anderson, R. F., Fleisher, M. Q., and LeHuray, A. P., 1989, Concentration, oxidation state, and particulate flux of uranium in the Black Sea: Geochimica et Cosmochimica Acta, v. 53, 2215-2224.

Arthur, M. A., Schlanger, S. O. T., and Jenkyns, H. C., 1987, The Cenomanian-Turonian Oceanic Anoxic Event, II. Paleoceanographic controls on organic-matter production and preservation: Geological Society, London, Special Publications 26, p. 401-420.

Bianchi, T. S., 2007, Hydrodynamics, *in* Bianchi, T. S., ed., Biogeochemistry of Estuaries, Oxford University Press, New York, p. 44.

Breit, G. N., and Wanty, R. B., 1991, Vanadium accumulation in carbonaceous rocks: A review of geochemical controls during deposition and diagenesis: Chemical Geology, v. 91, 83-97.

Brocks, J., Love, G. D., Summons, R. E., Knoll, A. H., Logan, G. A., and Bowden, S. A., 2005, Biomarker evidence for green and purple sulphur bacteria in a stratified Palaeoproterozic sea: Nature, v. 437, p. 866-870.

Brumsack, H.-J, 2006, The trace metal content of recent organic carbon-rich sediments: Implications for Cretaceous black shale formation: Palaeogeography, Palaeoclimatology, Palaeoecology, v. 232, p. 344-361.

Calvert, S. E., and Pedersen, T. F., 1993, Geochemistry of Recent oxic and anoxic marine sediments: Implications for the geological record: Marine Geology, v. 113, p. 67-88.

Chaillou, G., Anschutz, P., Lavaux, G., Schafer, J., and Blanc, G., 2002, The distribution of Mo, U, and Cd in relation to major redox species in muddy sediments of the Bay of Biscay: Marine Chemistry, v. 80, 41-59.

Crusius, J., Calvert, S. E., Pedersen, T., Sage, D., 1996, Rhenium and molybdenum enrichments in sediments as indicators of oxic, suboxic, and sulfidic conditions of deposition: Earth and Planetary Science Letters, v. 145, 65-78.

Dahl, T. W., Ruhl, M., Hammarlund, E. U., Canfield, D. E., Rosing, M. T., and Bjerrum, C. J., 2013, Tracing euxinia by molybdenum concentrations in sediments using handheld X-ray fluorescence spectroscopy: Chemical Geology, v. 360-361, p. 241-251.

Damste, J. S. S., and de Leeuw, J. W., 1990, Analysis, structure and geochemical significance of organically-bound sulphur in the geosphere: State of the art and future research: Organic Geochemistry, v. 16, no. 4-6, p. 1077-1101.

Damste, J. S. S., Rupstra, W. I. C., Kock-van Dalen, A. C., de Leeuw, J. W., and Schenck, P. A., 1989, Quenching of labile functionalized lipids by inorganic sulphur species: Evidence for the formation of sedimentary organic sulphur compounds at the early stages of diagenesis: Geochimica et Cosmochimica Acta, v. 53, p. 1343-1355.

Didyk, B. M, 1978, Organic geochemical indicators of palaeoenvironmental conditions of sedimentation: Nature, v. 272, p. 16.

Donovan, A. T., and Staerker, T. S., 2010, Sequence Stratigraphy of the Eagle Ford (Boquillas) Formation in the Subsurface of South Texas and Outcrops of West Texas: Gulf Coast Association of Geological Societies Transactions, v. 60, p. 861-899.

Donovan, A. T., Staerker, T. S., Pramudito, A., Li Weiguo, Corbett, M. J., Lowery, C. M., Romero, A. M., and Gardner, R. D., 2012, The Eagle Ford Outcrops of West Texas: A Laboratory for Understanding Heterogeneities within Unconventional Mudstone Reservoirs: GCAGS Journal, v. 1, 162-185.

Economides, M. J., Hill, A. D., Ehlig-Economides, C., and Zhu, D., 2013, Matrix Acidizing: Acid/Rock Interactions, *in* Economides, M. J., et al., eds., Petroleum Production Systems, Pearson Education.

Elder, W. P., 1989, Molluscan extinction patterns across the Cenomanian-Turonian Stage boundary in the western interior of the United States: Paleobiology, v. 15, no. 3, p. 299-320.

Eldrett, J. S., Minisini, D., and Bergman, S. C., 2014, Decoupling of the carbon cycle during Ocean Anoxic Event 2: Geology, v. 42, no. 7, p. 567-570.

Emerson, S. R., and Huested, S. S., 1991, Ocean anoxia and the concentrations of molybdenum and vanadium in seawater: Marine Chemistry, v. 34, 177-196.

Erickson, B. E., and Helz, G. R., 2000, Molybdenum(VI) speciation in sulfidic waters: Stability and lability of thiomolybdates: Geochimica et Cosmochimica Acta, v. 64, no. 7, 1149-1158.

Fernex, F., Fevrier, G., Benaim, J., and Arnoux, A., 1992, Copper, lead and zinc trapping in Mediterranean deep-sea sediments: probable coprecipitation with Mn and Fe: Chemical Geology, v. 98, 293-306.

Gale, A. S., Jenkyns, H. C., Kennedy, W. J., and Corfield, R. M., 1993, Chemostratigraphy versus biostratigraphy: data from around the Cenomanian - Turonian boundary: Journal of the Geological Society, v. 150, p. 29-32.

Gale, A. S., Smith, A. B., Monks, N. E. A., Young, J. A., Howard, A., Wray D. S., and Huggett, J. M., 2000, Marine biodiversity through the Late Cenomanian-Early Turonian: paleoceanographic controls and sequence stratigraphic biases: Journal of the Geological Society, London, v. 157, no. 4, p. 745-757.

Gardner, R. D., Pope, M. C., Wehner, M. P., and Donovan A. D., 2013, Comparative Stratigraphy of the Eagle Ford Group Strata in Lozier Canyon and Antonio Creek, Terrell County, Texas: GCAGS Journal, v. 2, p. 42-52.

Grice, K., Cao Changqun, Love, G. D., Bottcher, M. E., Twitchett, R. J., Grosjean, E., Summons, R. E., Turgeon, S. C., Dunning, W., and Jin Yugan, 2005, Photic Zone Euxinia During the Permian-Triassic Superanoxic Event: Science, v. 307, p. 706-709.

Grosjean, E., Adam, P., Connan, J., and Albrecht, P., 2004, Effects of weathering on nickel and vanadyl porphyrins of a Lower Toarcian shale of the Paris basin: Geochimica et Cosmochimica Acta, v. 68, no. 4, 789-804.

Guerra, K., Dahm, K., and Dundorf, S., 2011, Oil and Gas Produced Water Management and Beneficial Use in the Western United States, U.S. Department of the Interior Bureau of Reclamation Science and Technology Program Report 157, 113 p.

Hancock, J. M. and Kauffman, E. G., 1979, The great transgressions of the Late Cretaceous: Journal of the Geological Society, London, v. 136, p. 175-186.

Haq, B. U., Hardenbol, J., and Vail, P. R., 1987, Chronology of Fluctuating Sea Levels Since the Triassic: Science, v. 235, p. 1156-1167.

Hays, J. D., and Pitman, W. C. I., 1973, Lithospheric Plate Motion, Sea Level Changes and Climatic and Ecological Consequences: Nature, v. 246, p. 18-22.

Helz, G. R., Miller, C. V., Charnock, J. M., Mosselmans, J. F. W., Pattrick, R. A. D., Garner, C. D., Vaughan, D. J., 1996, Mechanism of molybdenum removal from the sea and its concentration in black shales: EXAFS evidence: Geochimica et Cosmochimica Acta, v. 60, no. 19, 3631-3642.

Hildred, G., Ratcliffe, K., and Schmidt, K., 2011, Application of Inorganic Whole-Rock Geochemistry to Shale Resource Plays: an Example from the Eagle Ford Shale, Texas: Houston Geological Society Bulletin, p. 31-38.

Huber, B. T., Hodell, D. A., and Hamilton, C. P., 1995, Middle-Late Cretaceous climate of the southern high latitudes: Stable isotopic evidence for minimal equator-to-pole thermal gradients: Geological Society of America Bulletin, v. 107, no. 10, p. 1164-1191.

Huber, B. T., Norris, R. D., and MacLeod, K. G., 2002, Deep-sea paleotemperature record of extreme warmth during the Cretaceous: Geology, v. 30, no. 2, p. 123-126.

Huerta-Diaz, M.A., and Morse, J. W., 1990, A Quantitative Method for Determination of Trace Metal Concentrations in Sedimentary Pyrite: Marine Chemistry, v. 29, 119-144.

Huerta-Diaz, M.A., and Morse, J. W., 1992, Pyritization of trace metals in anoxic marine sediments: Geochimica et Cosmochimica Acta, v. 56, 2681-2702.

Jarvis, I., Carson, G. A., Cooper, M. K. E., Hart, M. B., Leary, P. N., Tocher, B. A., Horne, D., and Rosenfeld, A., 1988, Microfossil Assemblages and the Cenomanian-Turonian (late Cretaceous) Oceanic Anoxic Event: Cretaceous Research, v. 9, p. 3-103.

Jenkyns, H. C., 1980, Cretaceous anoxic events: from continents to oceans: Journal of the Geological Society, v. 137, p. 171-188.

Jewell, P. W., 1993, Water-column stability, residence times, and anoxia in the Cretaceous North American seaway: Geology, v. 21, p. 579-582.

Kerr, A. C., 1998, Oceanic plateau formation: a cause of mass extinction and black shale deposition around the Cenomanian-Turonian boundary?: Journal of the Geological Society, London, v. 155, p. 619-626.

Klinkhammer, G. P., and Palmer, M. R., 1991, Uranium in the oceans: Where it goes and why: Geochimica et Cosmochimica Acta, v. 55, 1799-1806.

Koopmans, M. P., Koster, J., Van Kaam-Peters, H. M., Kenig, F., Schouten, S., Hartgers, W. A., de Leeuw, J. W., and Damste, J. S. S., 1996a, Diagenetic and catagenetic products of isorenieratene: Molecular indicators for photic zone anoxia: Geochimica et Cosmochimica Acta, v. 60, no. 22, p. 4467-4496.

Koopmans, M. P., Schouten, S., Kohnen, M. E., and Damste, J. S. S., 1996b, Restricted utility of aryl isoprenoids as indicators for photic zone anoxia: Geochimica et Cosmochimica Acta, v. 60, no. 23, p. 4873-4876.

Koopmans, M. P., de Leeuw, J. W., and Damste, J. S. S., 1997, Novel cyclised and aromatised diagenetic products of β-carotene in the Green River Shale: Organic Geochemistry, v. 26, no. 7/8, p. 451-466.

Lewan, M. D., and Maynard, J. B., 1982, Factors controlling enrichment of vanadium and nickel in the bitumen of organic sedimentary rocks: Geochimica et Cosmochimica Acta, v. 46, 2547-2560.

Liaaen-Jensen, S., 1978, Chemistry of carotenoid pigments, *in* Clayton, R. K., and Sistrom, W. R., eds., Photosynthetic Bacteria, Plenum Press, p 233-247.

Lock, B. E., and Peschier, L., 2006, Boquillas (Eagle Ford) Upper Slope Sediments, West Texas: Outcrop Analogs for Potential Shale Reservoirs: Gulf Coast Association of Geological Societies Transactions, v. 56, p. 491-508.

Markey, F., 2014, Examining Innovative Techniques for Matrix Acidizing in Tight Carbonate Formations to Minimize Damage to Equipment and Environment, Unconventional Resources Technology Conference, 25-27 August 2014, Denver.

McManus, J., Berelson, W. M., Klinkhammer, G. P., Hammond, D. E., and Holm, C., 2005, Authigenic uranium: relationship to oxygen penetration depth and organic carbon rain: Geochimica et Cosmochimica Acta, v. 69, no. 1, 95-108.

Melendez, I., Trinajstic, K, Ladjavardi, M., Greenwood, P., and Thompson, K., 2013, Biomarkers reveal the role of photic zone euxinia in exceptional fossil preservation: An organic geochemical perspective: Geology, v. 41, no. 2, p. 123-126.

Morford, J. L., and Emerson, S. R., 1999, The geochemistry of redox sensitive trace metals in sediments: Geochimica et Cosmochimica Acta, v. 63, no. 11/12, p. 1735-1750.

Morse, J. W., and Luther, G. W. I., 1999, Chemical influences on trace metal-sulfide interactions in anoxic sediments: Geochimica et Cosmochimica Acta, v. 63, no. 19/20, 3373-3378.

Pedersen, T. F., Vogel, J. S., and Southon, J. R., 1986, Copper and manganese in hemipelagic sediments at 21N, East Pacific Rise: Diagenetic contrasts: Geochimica et Cosmochimica Acta, v. 50, 2019-2031.

Pierce, J. D., 2014, U-Pb Geochronology of the Late Cretaceous Eagle Ford Shale, Texas; Defining Chronostratigraphic Boundaries and Volcanic Ash Source [M.S. thesis]: Austin, University of Texas, 157 p.

Pratt, L. M., 1985, Isotopic studies of organic matter and carbonate in rocks of the Greenhorn marine cycle, Fine-Grained Deposits and Biofacies of the Cretaceous Western Interior Seaway: Evidence of Cyclic Sedimentary Processes.

Romero, A. A. M., 2014, Subsurface and Outcrop Organic Geochemistry of the Eagle Ford Shale (Cenomanian-Coniacian) in West, Southwest, Central, and East Texas [Ph.D. thesis]: Norman, University of Oklahoma, 310 p.

Ruppel, S., Loucks, R., and Frebourg, G., 2012, Guide to field exposures of the Eagle Ford-equivalent Boquillas Formation and related Upper Cretaceous units in southwest Texas, Field seminar guidebook, 151 p.

Schaefle, J., Ludwig, B., Albrecht, P., and Ourisson, G., 1977, Hydrocarbures aromatiques d'origine geologique II: Nouveaux Carotenoides Aromatiques Fossiles: Tetrahedron Letters, v. 41, p. 3673-3676.

Schlanger, S. O., and Jenkyns, H. C., 1976, Cretaceous oceanic anoxic events: causes and consequences: Geologie en Mijnbouw, v. 55, no. 3-4, p. 179-184.

Schlanger, S. O., Jenkyns, H. C., and Premoli-Silva, I., 1981, Volcanism and vertical tectonics in the Pacific basin related to global Cretaceous transgressions: Earth and Planetary Science Letters 52: 435-449.

Schlanger, S. O., Arthur, M. A., Jenkyns, H. C., and Scholle, P. A., 1987, The Cenomanian-Turonian Oceanic Anoxic Event, I. Stratigraphy and distribution of organic carbon-rich beds and the marine d13C excursion: Geological Society, London, Special Publications, v. 26, p. 371-399.

Schwark, L., and Frimmel, A., 2004, Chemostratigraphy of the Posidonia Black Shale, SW-Germany II. Assessment of extent and persistence of photic-zone anoxia using aryl isoprenoid distributions: Chemical Geology, v. 206, p. 231-248.

Slingerland, R., Kump, L. R., Arthur, M. A., Fawcett, P. J., Sageman, B. B., and Barron, E. J., 1996, Estuarine circulation in the Turonian Western Interior seaway of North America: GSA Bulletin, v. 108, no. 7, p. 941-952.

Summons, R. E., and Powell, T. G., 1986, Chlorobiaceae in Palaeozoic seas revealed by biological markers, isotopes and geology: Nature, v. 319, p. 763-765.

Summons, R. E., and Powell, T. G., 1987, Identification of aryl isoprenoids in source rocks and crude oils: Biological markers for the green sulphur bacteria: Geochimica et Cosmochimica Acta, v. 51, p. 557-566.

Sullivan, P. J., and Yelton, J. L., 1988, An Evaluation of Trace Element Release Associated with Acid Mine Drainage: Environmental Geology and Water Science, v. 12, no. 3, 181 – 186.

Sun, Y.-Z., and Puttmann, W., 2000, The role of organic matter during copper enrichment in Kupferschiefer from the Sangerhausen basin, Germany: Organic Geochemistry, v. 31, 1143-1161.

Tinnin, B., and Hildred, G., 2013, Expanding the Application of Chemostratigraphy within Cretaceous Mudrocks: Estimating Total Organic Carbon and Paleoredox Facies using Major, Minor and Trace Element Geochemistry, Unconventional Resources Technology Conference.

Tribovillard, N., Riboulleau, A., Lyons, T., and Baudin, F., 2004, Enhanced trapping of molybdenum by sulfurized marine organic matter of marine origin in Mesozoic limestones and shales: Chemical Geology, v. 213, p. 385-401.

Tribovillard, N., Algeo, T. J., Lyons, T., and Riboulleau, A., 2006, Trace metals as paleoredox and paleoproductivity proxies: An update: Chemical Geology, v. 232, p. 12-32.

Vorlicek, T. P., and Helz, G. R., 2002, Catalysis by mineral surfaces: Implications for Mo geochemistry in anoxic environments: Geochimica et Cosmochimica Acta, v. 66, no. 21, 3679-3692.

Vorlicek, T. P., Kahn, M. D., Kasuya, Y., and Helz, G. R., 2004, Capture of molybdenum in pyrite-forming sediments: Role of ligand-induced reduction by polysulfides: Geochimica et Cosmochimica Acta, v. 68, no. 3, 547-556.

Wanty, R. B., and Goldhaber, M. B., 1992, Thermodynamics and kinetics of reactions involving vanadium in natural systems: Accumulation of vanadium in sedimentary rocks: Geochimica et Cosmochimica Acta, v. 56, 1471-1483.

Wehrli, B., and Stumm, W., 1989, Vanadyl in natural waters: Adsorption and hydrolysis promote oxygenation: Geochimica et Cosmochimica Acta, v. 53, 69-77.

Zheng, Y., Anderson, R. F., van Geen, A., and Kuwabara, J., 2000, Authigenic molybdenum formation in marine sediments: A link to pore water sulfide in the Santa Barbara Basin: Geochimica et Cosmochimica Acta, v. 64, 24, 4165-4178.

APPENDIX A

MOLECULAR STRUCTURES

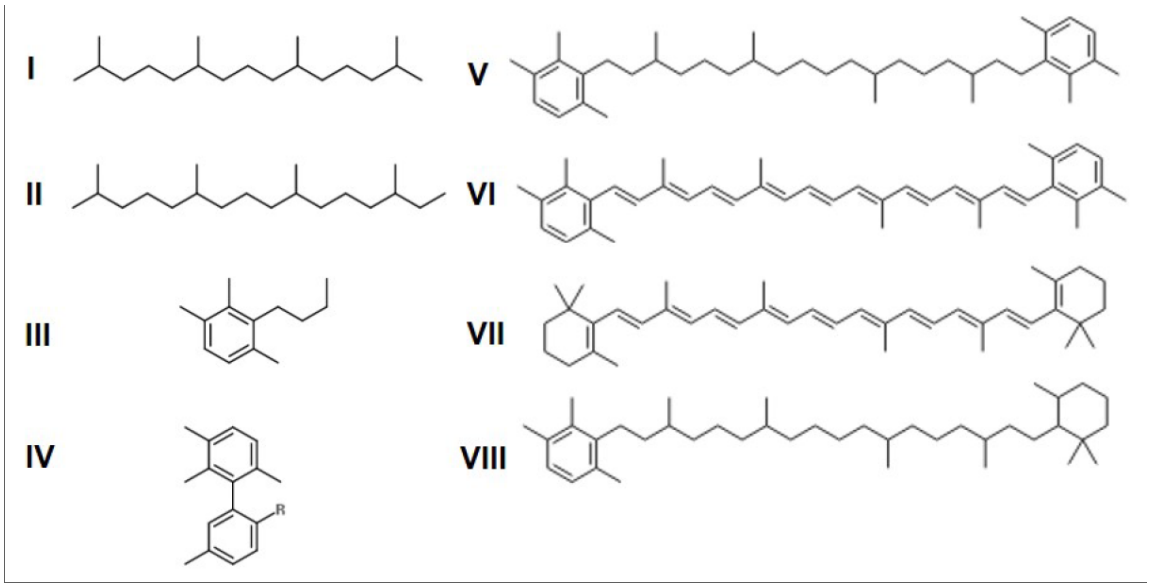

APPENDIX B

GSA DATA REPOSITORY SUPPLEMENTARY INFORMATION

The supplemental file is available in PDF form with this document.